Supporting Information for *Acta Phys. -Chim. Sin.* doi: 10.3866/PKU.WHXB202210003

多面体状 Cu_2O 修饰片状 BiOI 的 S 型异质结构筑及光催化水蒸气中 CO_2 转化性能研究

王吉超[1,3,*]，乔秀[1]，史维娜[2,*]，贺景[1]，陈军[1]，张万庆[1]

[1]河南科技学院化学化工学院，河南 新乡 453003

[2]新乡学院化学与材料工程学院，河南 新乡 453003

[3]郑州大学化学学院，郑州 450000

S-Scheme Heterojuntion of Cu_2O Polytope Modified BiOI Sheet for Efficient Visible-Light-Driven CO_2 Conversion under Water Vapor

Ji-Chao Wang [1,3,*], Xiu Qiao [1], Weina Shi [2,*], Jing He [1], Jun Chen [1], Wanqing Zhang [1]

[1] College of Chemistry and Chemical Engineering, Henan Institute of Science and Technology, Xinxiang 453000, Henan Province, China.

[2] School of Chemistry and Materials Engineering, Xinxiang University, Xinxiang 453000, Henan Province, China.

[3] School of Chemistry, Zhengzhou University, Zhengzhou 450000, China.

[*]Corresponding authors. Emails: shiweina516@163.com (W.S.); wangjichao@hist.edu.cn (J.-C.). Tel.: +86-18236123751 (W.S.); +86-373-3040148 (J.-C.).

S1 Characterization

The crystal structure and phase of as-prepared samples were measured by XRD using Cu K_α radiation (λ = 0.15406 nm) and its scanning range was from 10° to 80° with the 2θ. The chemical compositions and valence state were determined by XPS at room temperature with Al K_α radiation as the excitation source. HeI (21.2 eV) as monochromatic was adopted as a light source in UPS measurement. The optical properties of the obtained samples were determined in the wavelength range of 200 to 800 nm *via* a UV-Vis spectrometer. Lastly, a conventional three-electrode system was adopted in the measurement process of the photoelectrochemical spectroscopy, obtained by CHI660E workstation. For further exploring the transition states and intermediate media during the process of CO_2 conversion over the catalyst surface, the *in-situ* DRIFTS were measured using an infrared Fourier transform spectrometer (Nicolet iS50, TMO, USA). In the above test, the prepared samples should be degassed at 120 °C and placed in a specimen chamber.

S2 Photocatalytic performance tests

In the test process of photocatalytic performance, the visible-light source (λ > 400 nm) was provided by 300 xenon arc lamp with UV cutoff filter. The photocatalyst on FTO substate (2.0 × 2.0 cm^2) was placed on specific bracket inside the reactor. Before light began, the high pressure reactor should be washed by the CO_2 gas (99.999%) for several times. In last process of gas addition, the CO_2 reactant gas should firstly go through a water bubbler and then inject into reactor. In the offline analysis system about the gaseous products, two kinds columns (TDX-01 and Porapak-Q) should be adopted in the GC equipment with FID and GC-MS equipment with TCD, respectively. For exploring the other hydrocarbons, a capillary column (DB-FFAP) was also used in other GC with TCD. In blank tests for photocatalytic CO_2 conversion, the existence of catalysts and/or illumination was firstly studied under the same reaction conditions. And then, the photocatalytic activity in Ar atmosphere, instead of CO_2 atmosphere, was recorded to eliminate the disturbance of residual carbon on catalyst surface. No product was detected in above blank test, manifesting that the indispensable presence of both the irradiation and catalyst for the CO_2 conversion in water vapor.

Table S1 Main product yields for photocatalytic CO_2 reduction over BiOI/Cu_2O-1500 and BiOI/Cu_2O-1500m samples.

Catalyst	Photocatalytic activity (μmol·m^{-2})			
	CO	CH_4	H_2	O_2
BiOI/Cu_2O-1500	12.47	13.40	1.37	31.56
BiOI/Cu_2O-1500m	5.61	3.52	0.51	6.53

Table S2 Performance comparison of CO_2 conversion for the obtained BiOI/Cu_2O material and other reported catalysts

Catalyst	Catalytic activity	Catalytic condition	Reference
Ag-Cu_2O/ZnO	CO: 3.36 μmol·g^{-1}	UV-visible light 4 h irradiation	1
CdS/BiOI	CO: 3.32 μmol·g^{-1}	visible light 3 h irradiation	2
	CH_4: 0.54 μmol·g^{-1}		
In_2O_3/BiOI	CO: 11.98 μmol·g^{-1}·h^{-1}	visible light 4 h irradiation	3
	CH_4: 5.69 μmol·g^{-1}·h^{-1}	TEOA as sacrificial agent	
Bi_2WO_6-x/BiOI	CH_4: 18.32 μmol·g^{-1}	UV-Vis light 8 h irradiation	4
Cu_2O@Cu@UiO-66-NH_2	CO: 20.9 μmol·g^{-1}·h^{-1}	visible light 5 h irradiation	5
	CH_4: 8.3 μmol·g^{-1}·h^{-1}	TEOA as sacrificial agent	
Co-MOF/Cu_2O	CO: 3.83 μmol·g^{-1}·h^{-1}	visible light 4 h irradiation	6
Ag-Cu_2O/TiO_2	CO: 13.19 μmol·g^{-1}·h^{-1}	simulated sunshine irradiation	7
	CH_4: 1.74 μmol·g^{-1}·h^{-1}		
g-C_3N_4/BiOI/RGO	CO: 21.85 μmol·g^{-1}	visible light 8 h irradiation	8
Cu_2O/BiOI	CH_3OH: 609.05 μmol·g^{-1}	UV-Vis irradiation 0.1 mol·L^{-1} NaOH with	9
	C_2H_5OH: 273.96 μmol·g^{-1}	adding CO_2 (g)	
BiOI/Cu_2O	CO: 10.61 μmol·g^{-1}·h^{-1}	visible light 11 h irradiation	This work
	CH_4: 6.15 μmol·g^{-1}·h^{-1}		
	O_2: 16.55 μmol·g^{-1}·h^{-1}		
	H_2: 1.70 μmol·g^{-1}·h^{-1}		

Table S3 Binding energy and band gap of the BiOI, Cu_2O and BiOI/Cu_2O-1500 samples by XPS and DRS measurements.

Sample	Bi 4*f* (eV)	Cu 2*p* (eV)	VB (eV)	E_g/eV
BiOI	159.6	–	1.9	1.8
Cu_2O	–	931.8	0.8	2.0
BiOI/Cu_2O-1500	158.9	932.7	–	–

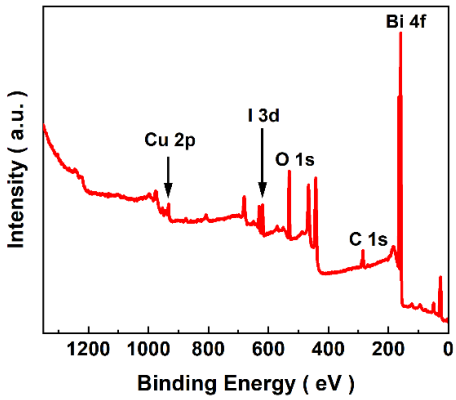

Fig. S1 Survey XPS spectrum of BiOI/Cu_2O-1500 sample.

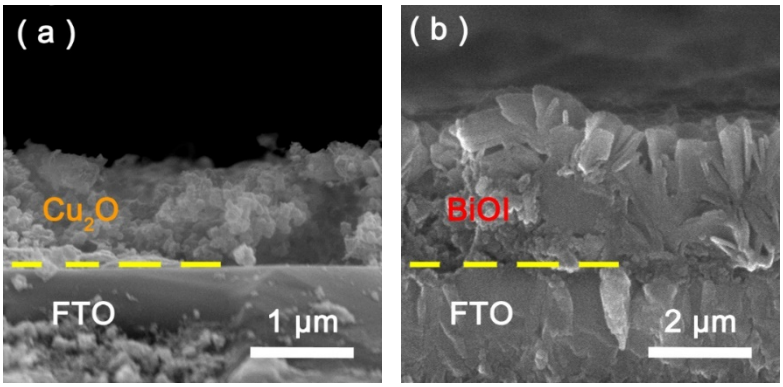

Fig. S2 SEM image of Cu_2O(a) and BiOI(b) samples.

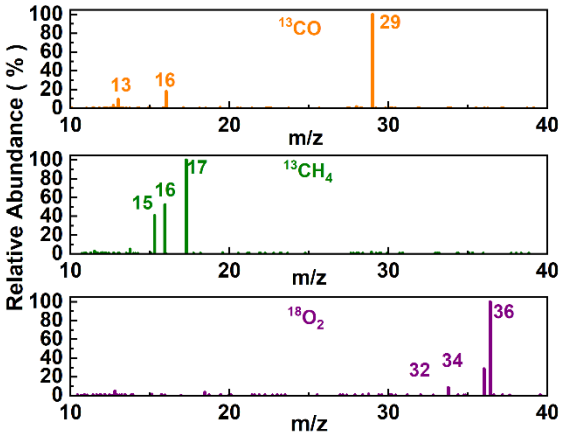

Fig. S3 Mass spectra of ^{13}CO, $^{13}CH_4$ and $^{18}O_2$ products over the BiOI/Cu_2O-1500 photocatalyst for CO_2 photoreduction.

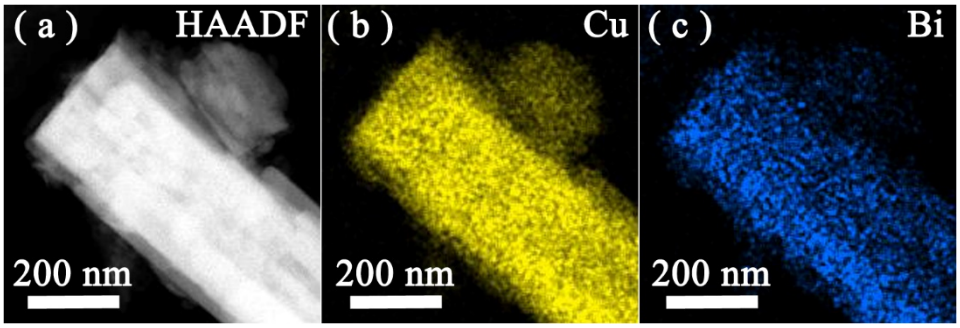

Fig. S4 HAADF (a) and EDX mapping images (b: Cu element, c: Bi element) of the BiOI/Cu_2O-2100 sample.

Firstly, the BiOI component exhibited the nanosheet morphology with thickness of approximately 10 nm based on the SEM images (Fig. 2a). With the increase of electrodeposition cycles for Cu_2O, the sheet thickness distinctly increased, reaching approximately 84 nm for the BiOI/Cu_2O-2100 sample (Fig. 2g). The distribution of Cu element in Fig. S3 covered the whole BiOI nanosheet, which indicated that Cu_2O grew on the whole surface of BiOI nanosheet. Secondly, based on the photocatalytic performance and mechanism, the oxidation reaction occurred on the surface of BiOI component in the composite. As shown in Fig. 3a, the photocatalytic activity of BiOI/Cu_2O-1800 and BiOI/Cu_2O-2100 were lower than that of BiOI/Cu_2O-1500, and the difference between hole quantity (N_{Ox}) and electron quantity (N_{Red}) gradually increased, and it was caused by the declined efficiency of H_2O oxidation reaction. Hence, the decreased photocatalytic activity was caused by the coverage of BiOI with Cu_2O electrodeposition.

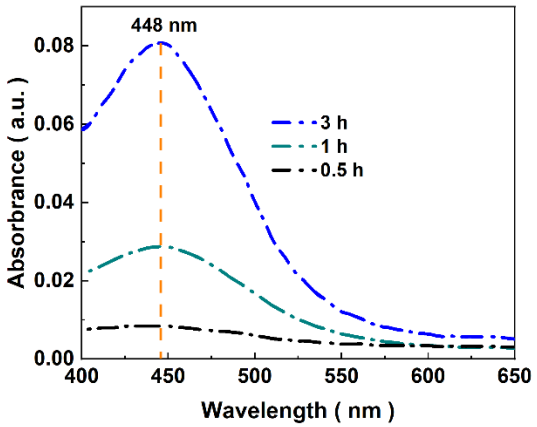

Fig. S5 UV-Vis absorption spectra with *o*-tolidine as peroxide indicator for the BiOI/Cu_2O-1500 catalyst.

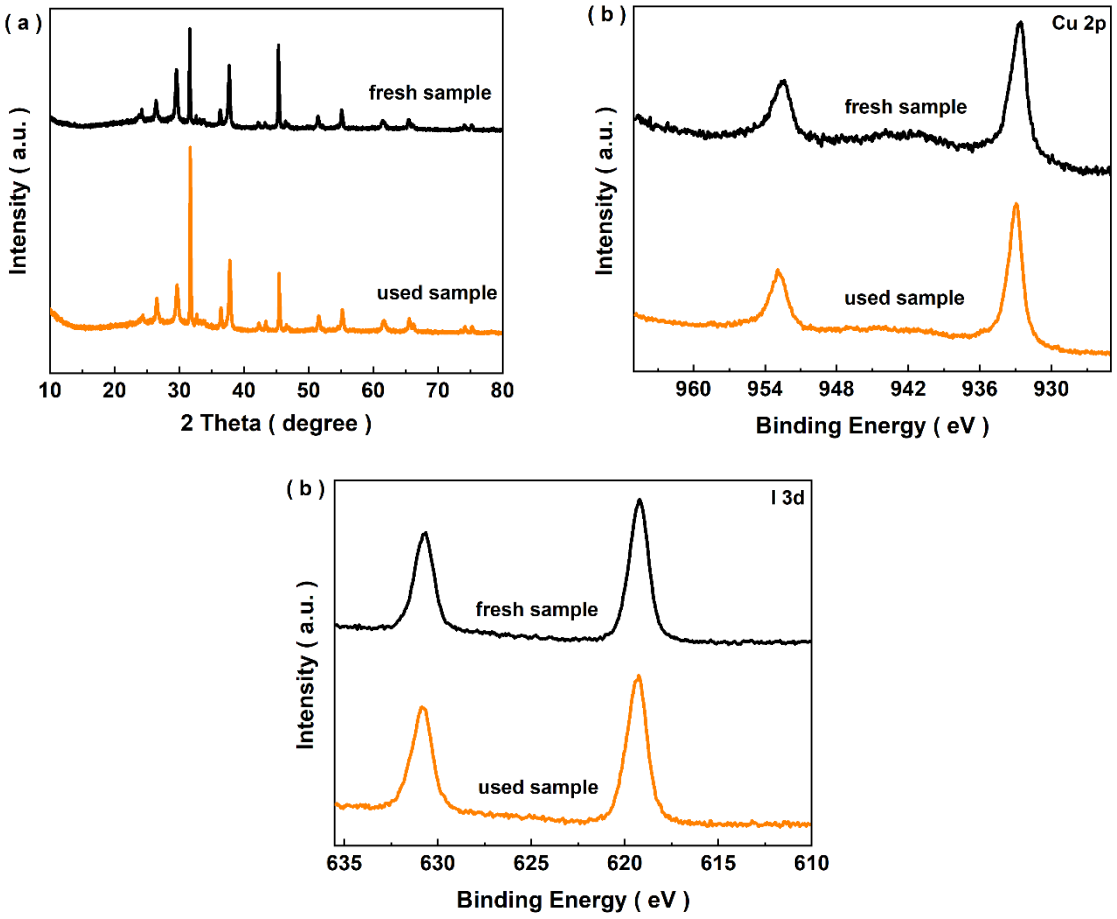

Fig. S6 XRD (a) and XPS (b, c) spectra of BiOI/Cu_2O-1500 photocatalyst before/after cycling experiment (b. Cu 2*p* and c. I 3*d*).

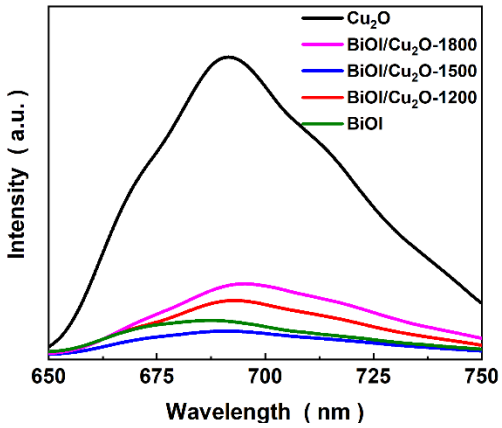

Fig. S7 PL spectra for BiOI, Cu_2O and BiOI/Cu_2O composites.

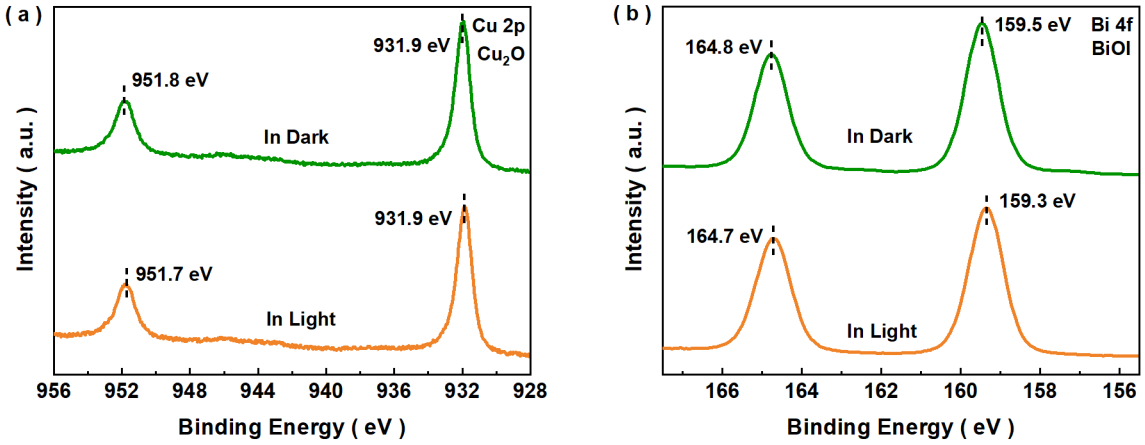

Fig. S8 *In situ*-XPS spectra of BiOI and Cu_2O in dark and light (a. Cu 2*p* and b. Bi 4*f*). The characteristic peaks of Cu 2*p* and Bi 4*f* for the bare BiOI and Cu_2O samples in light slightly shifted toward lower energy compared with those in dark. It was due to that the CB of Cu_2O and BiOI mainly consisted of Cu *sp* and Bi *sp* orbits and the electrons were excited from VB to CB under illumination [10,11].

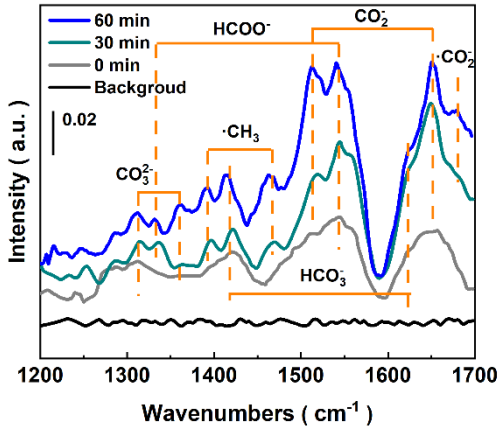

Fig. S9 The *in-situ* DRIFTS of BiOI/Cu_2O-1500 sample. Several characteristic peaks of CO_3^{2-} (1317 and 1365 cm^{-1}), CO_2^- (1651 and 1516 cm^{-1}), HCO_3^- (1625 and 1422 cm^{-1}) and $HCOO^-$ (1542 and 1339 cm^{-1}) species appeared, and the peak intensities gradually increased with increasing the light irradiation time [12–17]. It was demonstrated that $HCOO^-$ was an important intermediate during the process of photocatalytic CO_2 reduction to CO, which was consistent with previous reports [16,17]. Three peaks of $\cdot CH_3$ (1457 and 1389 cm^{-1}) and $\cdot CO_2^-$ (1678 cm^{-1}) were identified [18,19], which indicated the production of CH_4.

References

(1) Zhang, F.; Li, Y.-H.; Qi, M.-Y.; Tang, Z.-R.; Xu, Y.-J. *Appl. Catal. B: Environ.* **2020,** *268*, 118380. doi: 10.1016/j.apcatb.2019.118380

(2) Zhou, R.-H.; Wei, Z.-H.; Li, Y.-Y.; Li, Z.-J.; Yao, H.-C. *J. Mater. Res.* **2019,** *34* (23), 3907. doi: 10.1557/jmr.2019.354

(3) Sun, N.; Zhou, M.; Ma, X.; Cheng, Z.; Wu, J.; Qi, Y.; Sun, Y.; Zhou, F.; Shen, Y.; Lu, S. *J. CO_2 Util.* **2022,** *65*, 102220. doi: 10.1016/j.jcou.2022.102220

(4) Kong, X. Y.; Lee, W. Q.; Mohamed, A. R.; Chai, S.-P. *Chem. Eng. J.* **2019,** *372*, 1183. doi: 10.1016/j.cej.2019.05.001

(5) Wang, S.-Q.; Zhang, X.-Y.; Dao, X.-Y.; Cheng, X.-M.; Sun, W.-Y. *ACS Appl. Nano Mater.* **2020,** *3* (10), 10437. doi: 10.1021/acsanm.0c02312

(6) Dong, W.-W.; Jia, J.; Wang, Y.; An, J.-R.; Yang, O.-Y.; Gao, X.-J.; Liu, Y.-L.; Zhao, J.; Li, D.-S. *Chem. Eng. J.* **2022,** *438*, 135622. doi: 10.1016/j.cej.2022.135622

(7) Wang, X.; Jiang, Z.; Chen, H.; Wang, K.; Wang, X. *J. Alloys Compd.* **2022,** *896*, 163030. doi: 10.1016/j.jallcom.2021.163030

(8) Hu, X.; Hu, J.; Peng, Q.; Ma, X.; Dong, S.; Wang, H. *Mater. Res. Bull.* **2020,** *122*, 110682. doi: 10.1016/j.materresbull.2019.110682

(9) Cai, J.; Xiao, Y.; Tursun, Y.; Abulizi, A. *Mater. Sci. Semicond. Process.* **2022,** *149*, 106891. doi: 10.1016/j.mssp.2022.106891

(10) Ye, L.; Jin, X.; Ji, X.; Liu, C.; Su, Y.; Xie, H.; Liu, C. *Chem. Eng. J.* **2016,** *291*, 39. doi: 10.1016/j.cej.2016.01.032

(11) Zhang, M.; Wang, J.; Xue, H.; Zhang, J.; Peng, S.; Han, X.; Deng, Y.; Hu, W. *Angew. Chem. Int. Ed.* **2020,** *59* (42), 18463. doi: 10.1002/anie.202007680

(12) Li, F.; Yue, X.; Zhang, D.; Fan, J.; Xiang, Q. *Appl. Catal. B* **2021,** *292*, 120179. doi: 10.1016/j.apcatb.2021.120179

(13) Han, C.; Zhang, R.; Ye, Y.; Wang, L.; Ma, Z.; Su, F.; Xie, H.; Zhou, Y.; Wong, P. K.; Ye, L. *J. Mater. Chem. A* **2019,** *7*, 9726. doi: 10.1039/c9ta01061k

(14) Jiang, Z.; Sun, H.; Wang, T.; Wang, B.; Wei, W.; Li, H.; Yuan, S.; An, T.; Zhao, H.; Yu, J.; Wong, P. K. *Energy Environ. Sci.* **2018,** *11* (9), 2382. doi: 10.1039/c8ee01781f

(15) He, Y.; Li, C.; Chen, X.-B.; Shi, Z.; Feng, S. *ACS Appl. Mater. Interfaces* **2022,** *14*, 28977. doi: 10.1021/acsami.2c06993

(16) Jin, L.; Shaaban, E.; Bamonte, S.; Cintron, D.; Shuster, S.; Zhang, L.; Li, G.; He, J. *ACS Appl. Mater. Interfaces* **2021,** *13* (32), 38595. doi: 10.1021/acsami.1c09119

(17) Yang, P.; Wang, R.; Zhuzhang, H.; Titirici, M.-M.; Wang, X. *ACS Catal.* **2020,** *10* (21), 12706. doi: 10.1021/acscatal.0c03607

(18) Chen, C.; Wang, T.; Yan, K.; Liu, S.; Zhao, Y.; Li, B. *Inorg. Chem. Front.* **2022,** *9* (18), 4753. doi: 10.1039/d2qi01155g

(19) Li, N.; Wang, B.; Si, Y.; Xue, F.; Zhou, J.; Lu, Y.; Liu, M. *ACS Catal.* **2019,** *9* (6), 5590. doi: 10.1021/acscatal.9b00223